

Article

Synthesis, Characterization, and Antibacterial Potential of Poly(*o*-anisidine)/BaSO₄ Nanocomposites with Enhanced Electrical Conductivity

Mirza Nadeem Ahmad ¹, Sohail Nadeem ^{2,*}, Raya Soltane ^{3,4}, Mohsin Javed ², Shahid Iqbal ^{5,*}, Zunaira Kanwal ¹, Muhammad Fayyaz Farid ¹, Sameh Rabea ⁶, Eslam B. Elkaeed ⁶, Samar O. Aljazzar ⁷, Hamad Alrbyawi ⁸ and Walid F. Elkhatib ^{9,10}

¹ Department of Applied Chemistry, Government College University, Faisalabad 38030, Pakistan

² Department of Chemistry, School of Science, University of Management and Technology, Lahore 54770, Pakistan

³ Department of Basic Sciences, Adham University College, Umm Al-Qura University, Makkah 21955, Saudi Arabia

⁴ Department of Biology, Faculty of Sciences, Tunis El Manar University, Tunis 1068, Tunisia

⁵ Department of Chemistry, School of Natural Sciences (SNS), National University of Science and Technology (NUST), H-12, Islamabad 46000, Pakistan

⁶ Department of Pharmaceutical Sciences, College of Pharmacy, Almaarefa University, Riyadh 13713, Saudi Arabia

⁷ Department of Chemistry, College of Science, Princess Nourah Bint Abdulrahman University, P.O. Box 84428, Riyadh 11671, Saudi Arabia

⁸ Pharmaceutics and Pharmaceutical Technology Department, College of Pharmacy, Taibah University, Medina 42353, Saudi Arabia

⁹ Microbiology and Immunology Department, Faculty of Pharmacy, Ain Shams University, African Union Organization St., Abbassia, Cairo 11566, Egypt

¹⁰ Department of Microbiology & Immunology, Faculty of Pharmacy, Galala University, P.O. Box 46000, Suez 43511, Egypt

* Correspondence: sohail.nadeem@umt.edu.pk (S.N.); shahidgcs10@yahoo.com (S.I.)

Citation: Ahmad, M.N.; Nadeem, S.; Soltane, R.; Javed, M.; Iqbal, S.; Kanwal, Z.; Farid, M.F.; Rabea, S.; Elkaeed, E.B.; Aljazzar, S.O.; et al. Synthesis, Characterization and Antibacterial Potential of Poly(*o*-anisidine)/BaSO₄ Nanocomposites with Enhanced Electrical Conductivity. *Processes* **2022**, *10*, 1878. <https://doi.org/10.3390/pr10091878>

Academic Editors: Iliyan Ivanov and Stanimir Manolov

Received: 29 July 2022

Accepted: 14 September 2022

Published: 16 September 2022

Publisher's Note: MDPI stays neutral with regard to jurisdictional claims in published maps and institutional affiliations.



Copyright: © 2022 by the authors. Licensee MDPI, Basel, Switzerland. This article is an open access article distributed under the terms and conditions of the Creative Commons Attribution (CC BY) license (<https://creativecommons.org/licenses/by/4.0/>).

Abstract: The poly(*o*-anisidine)/BaSO₄ nanocomposites were prepared by oxidative polymerization of *o*-anisidine monomer with BaSO₄ filler for the potential antibacterial properties of the composite materials. To achieve the optimal and tunable properties of the nanocomposites, the ratio of BaSO₄ filler was changed at the rates of 1%, 3%, 5%, 7%, and 10% with respect to matrix. Different analytical techniques, i.e., FTIR and UV-visible spectroscopy, were employed for functional identification and optical absorption of the poly(*o*-anisidine)/BaSO₄ nanocomposites. The FTIR data revealed the significant interaction between POA and BaSO₄, as well as the good absorption behavior of the UV-visible spectra. The conducting properties were controllable by varying the load percentage of the BaSO₄ filler. Furthermore, different bacterial strains, i.e., *Pseudomonas aeruginosa* (Gram-negative) and *Staphylococcus aureus* (Gram-positive), were used to evaluate the antibacterial activity of the POA/BaSO₄ nanocomposites. The largest zones of inhibition 0.8 and 0.9 mm were reached using 7% and 10% for *Staphylococcus aureus* and *Pseudomonas aeruginosa*, respectively.

Keywords: nanocomposites; antibacterial; electrical conductivity; BaSO₄; polymerization

1. Introduction

The development of nanomaterials has been a useful and important task during the last fifteen years. These nanomaterials have original multifunctionalities, which make them very helpful products in a variety of industries. The nanocomposites are classified into structural and functional materials. Structural nanocomposites focus on the improvement of mechanical properties due to the addition of nanoparticles, while for the

functional ones, the presence of nanoparticles adds extra functionalities to the polymer, such as electrical conductivity, special optical properties, antimicrobial features, and many more. The hybrid nanomaterials consist of organic–inorganic components, e.g., organic polymer matrix and inorganic filler, and have potential applications as antimicrobial agents, biocompatible materials, sensors, and electrical devices. Moreover, they are utilized as high-value coatings in gas separation, ultra- and nanofiltration, and corrosion prevention, as well as in artificial membranes [1–3]. In addition, they can be used as catalysts, toxic-compound adsorbents, biomaterials, and information display materials with specialized optical, magnetic, and electrical capabilities [4–6].

These nanomaterials offer unique properties due to the fact that their components have a different nature to prepare some tailor-made novel nanomaterials [7–10]. In particular, the composites made by adding multi-walled carbon nanotubes to thin layers of poly(3,4-ethylenedioxythiophene) and poly(4-styrenesulfonate) exhibited intriguing characteristics regarding the interdependence of electrical properties towards the large temperature range [11]. Thus, the inorganic and organic species interact at a molecular level at the nanoscopic range. Similarly, Mt-PS-BZO-PANI hybrid composites showed valuable luminescence properties [12]. Moreover, polyurethane (PU) and poly(hydroxyethyl methacrylate) composited with poly(titanium oxide) showed excellent viscoelastic and thermophysical properties [13]. The ability of these organic–inorganic hybrid materials to blend the heterogeneous properties of inorganic–organic components in a single material is its key benefit. In recent years, nanomaterials have offered one of the most interesting developments in the subject of materials chemistry [14–16].

The conducting polymer is one of a new class of polymers that are being used for a variety of applications. The merging of different unique properties, such as the chemical, electrical, and electrochemical properties of these polymers, may cause them to be used in several scientific applications [17–20]. Polyaniline has the unique property to coordinate with metallic ions, which provides the multi-metallic system and also prepares the nanocomposite materials with some other species. Polyaniline and its derivatives have achieved considerable attention over the last few years due to their conducting properties. The electro-active characteristics of polyaniline films, in particular, have been determined useful for the development of batteries, electrochromic displays, and microelectronics devices. Poly(*o*-anisidine) exhibits some interesting and unique properties [21–24]. Poly(*o*-anisidine) was found to have greater solubility compared with polyaniline in some organic solvents as it has a low boiling point while maintaining its crystalline property. This is very important because this polyaniline derivative can be used in technological applications [25–29].

Polymeric nanocomposites are modern and superior composites that are obtained from nanoparticles and the polymeric matrix, in which NPs are covered by polymers; through this, a core-shell arrangement can be developed [30]. Due to the particular shape, chemical nature, and exceptional structure of polymers, nanoparticles can be spread in a polymer matrix in the best and unique shapes. As a result of covering nanoparticles and their functionalization, the Van der Waals forces among NPs become reduced and the distribution of NPs in the matrix is improved and amplified [31,32]. The importance of polymer nanocomposites lies in the fact that polymers are always preferred for the covering of nanoparticles. On the other hand, appropriate functional groups in polymer structures can be used as reaction sites to organize the one-pot synthesis of nanocomposites [33,34].

Polymeric materials can be extensively employed in industries because of their lightweight and their simplicity of preparation, in addition to their elastic properties. Nevertheless, these materials have several drawbacks, such as their small modulus as well as potency compared to ceramics and metals [35]. Thus, to improve the mechanical properties, a very useful and valuable approach can be the addition of fibers, platelets, particles, or whiskers into such polymeric materials as reinforcements. The polymeric materials are composited with other filler materials to tune the properties of the materials, such as the

temperature resistance, impact opposition, mechanical strength, fire or flame resistance, gas permeability, conductivity, and microbial resistance [36].

Due to the addition of reinforcements or filler materials to a wide range of polymer resins, their unique properties have greatly been improved. This is a great example of polymer-matrix nanocomposites acting as eco-friendly systems. Furthermore, the latest information on nano-industries' nanomaterials showed complete and effective applications in the form of polymer nanocomposites and has been successfully reported [31,37]. Moreover, the barium sulfate has versatile applications and can be utilized as an antibacterial agent, a paint, a film, a fiber, and a luminescence material, and for photocatalysis [38–41]. Consequently, the versatile properties of barium-sulfate-nanocomposite materials proved their widespread applications in every field. Thus, there exists a big and wonderful demand for such hybrid materials. Generally, these hybrid materials, based on organic polymers, have many advantages, such as good processability, long-term stability, and wonderful optical, electronic, and catalytic as well as magnetic properties [42,43]. Thus, the resulting nanocomposites could offer numerous applications in different fields, for example, antibacterial, optoelectronics, electrical devices, sensors, etc. [44]. Moreover, barium-sulfate nanoparticles show antibacterial properties due to its small size, greater surface area, and high penetration power to inhibit the growth of bacteria [43]. The barium-sulfate nanoparticles not only exhibit the antimicrobial properties towards the nanocomposite but also control the electrical conductivity of the materials. Therefore, the antibacterial properties of BaSO₄ nanoparticles as filler and conducting properties of the poly(*o*-anisidine) matrix were combined to obtain novel composite materials with bactericidal and conducting properties, and for biomedical and sensor applications.

2. Material and Methods

For the present research work, all the chemicals, such as ammonium persulfate [(NH₄)₂S₂O₈], *o*-anisidine monomer as an oxidant, diaminodiphenylamine (DDPA), HCl/H₂SO₄, DI water, barium chloride, and ammonium sulfate, were procured from the Sigma Aldrich company (St. Louis, MI, USA). They were chemicals of the analytical and research grade, and they were utilized directly.

2.1. Preparation of Poly(*o*-anisidine)

Using a chemical oxidative approach, the *o*-anisidine was polymerized into poly(*o*-anisidine) (Figure 1). Two solutions were prepared and named solution A and solution B using the conventional process. By combining 3 g of monomer with 10 mL of 1 M HCl, solution A was created. Then, with magnetic stirring, solution A was added to an ice bath. The next step was to create solution B, which was made by combining 4 g of ammonium persulfate with 10 mL of 1 M HCl and keeping it in an ice bath. Solution B was added dropwise in solution A, which was already constantly stirred. The reaction contents were continuously stirred for 2 h. After that, it was left undisturbed overnight. The bluish-green suspension was prepared, which was subjected to centrifugation for isolation and purification. The material was isolated and washed with deionized water three times for better purification. Finally, the material was dried for 6 h at 80 °C in an electric oven and we proceeded with the characterization [17].

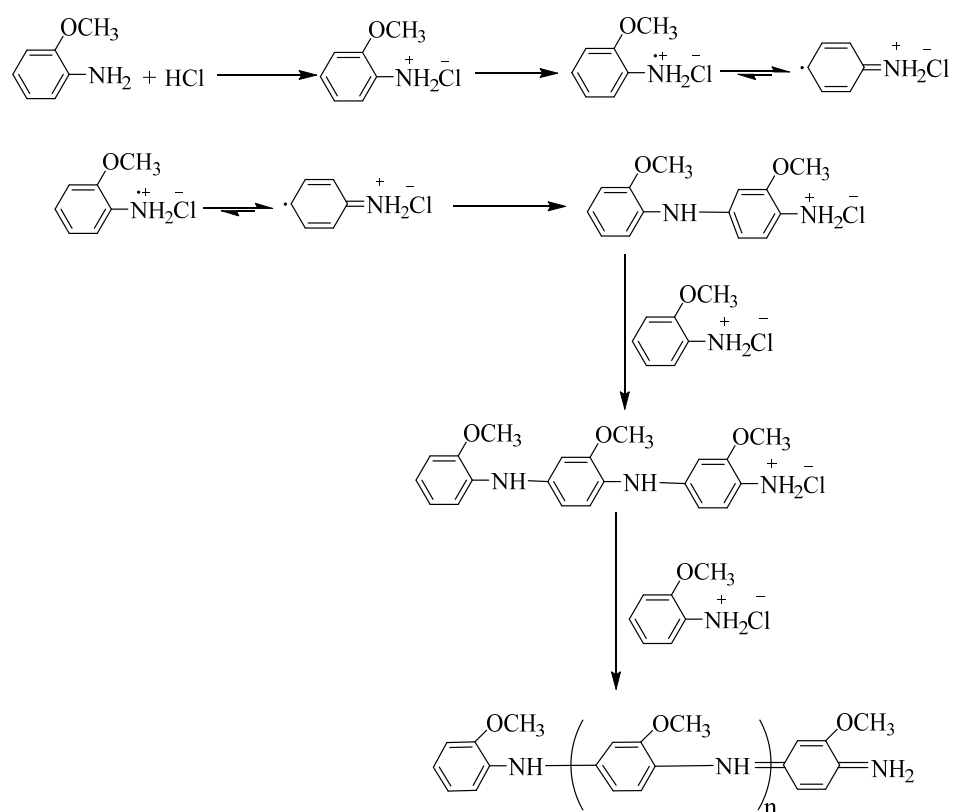


Figure 1. Proposed scheme for polymerization of *o*-anisidine.

2.2. Preparation of Barium-Sulfate Nanoparticles

BaSO₄ nanoparticles were prepared by using the method already reported by Ahmad et al. [44]. The 20 mL of the BaCl₂ (0.5 M) solution, along with 20 mL absolute ethanol, was taken in a conical flask. Then, the (NH₄)₂SO₄ solution (0.1 M) was prepared in distilled water. Then, the ammonium-sulfate solution was added dropwise to the conical flask containing the barium-chloride solution for 20 min with constant stirring at 25 °C. Afterwards, the gelatinous white barium-sulfate nanoparticles were formed, which were centrifuged to separate them from each other. Distilled water and ethanol were used to wash the item multiple times. Finally, the material was dried in an electric oven at 120 °C for 12 h. The dried material was collected to obtain the barium-sulfate nanoparticles.

2.3. Synthesis of Poly(*o*-anisidine)/BaSO₄ Nanocomposite

The preparation of the poly(*o*-anisidine)/BaSO₄ nanocomposites was carried out by following the method of poly(*o*-anisidine) polymerization. Two solutions were prepared, which were designated as solution A and solution B. For solution A, 0.246 g of *o*-anisidine monomer was added in 20 mL of HCl (1 M), along with 0.026 g of the DDPA and BaSO₄ nanoparticles. The load percentage of the BaSO₄ nanoparticles was changed for different composites (1, 3, 5, 7, and 10), as shown in Table 1. Then, solution A was sonicated for 10 min and placed to stir in an ice bath. Additionally, 20 mL of HCl and 0.246 g of APS were combined to create solution B (1 M). After that, solution B was continuously stirred into solution A while being introduced dropwise in an ice bath. The mixture was stirred for 2 h and kept overnight for stabilization. The greenish suspension was obtained and we proceeded to the centrifugation. The material was separated and washed with distilled water three times. Then, the material was dried in an electric oven at 80 °C for 6 h [17]. Similarly, other composites were prepared by varying the percentage of the BaSO₄ nanofiller according to the above method. Finally, the materials were collected and subjected to the characterization.

Table 1. Scheme for nanocomposite preparation.

| Sr. No. | <i>o</i> -anisidine Monomer | BaSO ₄ NPs | % of BaSO ₄ NPs |
|---------|-----------------------------|-----------------------|----------------------------|
| 1 | 0.246 g | 0 g | 0% |
| 2 | 0.246 g | 0.0024 g | 1% |
| 3 | 0.246 g | 0.0073 g | 3% |
| 4 | 0.246 g | 0.0123 g | 5% |
| 5 | 0.246 g | 0.0172 g | 7% |
| 6 | 0.246 g | 0.0246 g | 10% |

2.4. Characterization

The samples were characterized by various analytical techniques, as mentioned below.

2.4.1. FTIR Spectroscopic Studies

For the FTIR spectroscopic studies, the Agilent carrying 630 spectrometers was used to conduct the FTIR analysis of the poly(*o*-anisidine)/BaSO₄ nanocomposites. The sample discs were prepared by using KBr powder and dried to remove any moisture at 80 °C in an electric oven. Then, the samples were analyzed by the FTIR spectrometer in the wave-number range of 400–4000 cm⁻¹.

2.4.2. UV-Visible Spectroscopy

The UV-visible spectroscopic study of the poly(*o*-anisidine)/BaSO₄ nanocomposites was carried out using the Shimadzu double-beam spectrophotometer. The samples were prepared by dispersing 1 mg of the composite in 5 mL of distilled water. Then, the samples were scanned in the wavelength range of 200–800 nm.

2.4.3. TEM Analysis

On the H-7650 (Hitachi, Tokyo, Japan), running at an acceleration voltage of 100 kV, the TEM examination was performed.

2.4.4. Conductivity Measurement

The CyberScan PC 510 conductivity meter was used to conduct the conductivity measurement of the poly(*o*-anisidine)/BaSO₄ nanocomposites. The samples were prepared by dispersing 1 mg of the composite in 5 mL of distilled water. Then, the dispersion was used for the measurement of electrical conductivity by the conductivity meter.

2.4.5. Antibacterial Activity

The antibacterial capability of the poly(*o*-anisidine)/BaSO₄ nanocomposites was assessed using the disc-diffusion technique. Antibacterial testing was carried out by using the disc-diffusion method. Bacterial growth was carried out by using the nutrient-growth agar method. Only Gram-negative bacteria (*Pseudomonas aeruginosa*) were used in the MacConkey agar. *Pseudomonas aeruginosa* can grow on MacConkey but *Staphylococcus aureus* cannot grow on MacConkey. The media were autoclaved, chilled, and deposited in petri plates for 41 min. Forty-one minutes later, hardened agar plates were covered with a fresh inoculum (20 mL) of bacteria cultures. The UVAS diagnostic lab provided bacterial cultures. Every plate contained sterile paper discs dipped in various suspensions of the POA/BaSO₄ nanocomposites. For 24 h, the agar plates were incubated at 37 °C (310 K). The zones of inhibition were studied following a 24-hour incubation period. The magnitude of the presence or absence of growth inhibition zones was used to determine the sensitivity and resistance of bacteria in sensitivity tests.

3. Results and Discussion

The synthesized poly(*o*-anisidine)/BaSO₄ nanocomposites were characterized by various techniques, as mentioned above. Six samples were prepared, in which one was the pure polymer and other five were nanocomposites with BaSO₄ nanoparticles (1%, 3%, 5%, 7%, and 10%). The barium-sulfate nanoparticles were characterized by powder XRD and the average particle size was 25.26 nm, as reported by Ahmad et al. [44]. The composites were further analyzed by using the following analytical techniques.

3.1. FTIR Spectroscopic Studies

The FTIR analysis of the poly(*o*-anisidine)/BaSO₄ nanocomposites was carried out to determine the structural changes in the material. The C=C stretching mode of the quinoid ring appeared at 1591 cm⁻¹, which was attributed to the stretching vibration of the *o*-methoxy group. The poly(2-methoxy aniline) signal appeared at 3379 cm⁻¹, which was attributed to the N-H stretching mode. The C=C stretching modes of the benzenoid ring appeared at 1469, 1206, and 1032 cm⁻¹, which were attributed to the stretching vibration of the *o*-methoxy group. The methoxy band clearly indicated the existence of poly(*o*-methoxy aniline) in the spectra. The spectrum in Figure 2b shows the addition of 1% of the BaSO₄ nanoparticles in the poly(*o*-anisidine) matrix at 2837 cm⁻¹, demonstrating the interaction of the poly(*o*-anisidine) with the BaSO₄ that appeared as the peak was deeper and wider.

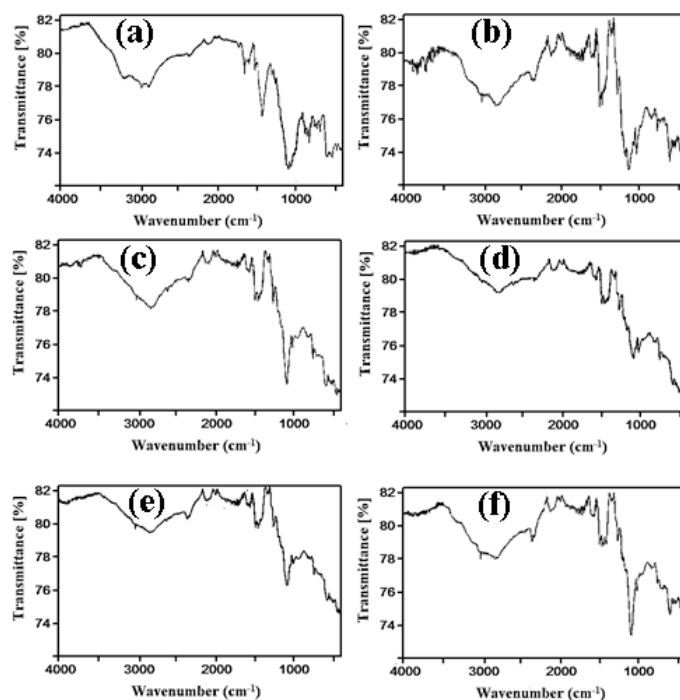


Figure 2. FTIR spectra of (a) pure POA, (b) 1% of POA/BaSO₄, (c) 3% of POA/BaSO₄, (d) 5% of POA/BaSO₄, (e) 7% of POA/BaSO₄, and (f) 10% of POA/BaSO₄.

The peak that appeared at 2837 cm⁻¹ with the addition of 3 percent of the BaSO₄ nanoparticles in the poly(*o*-anisidine) matrix was practically the same as in the 1 percent, indicating that the 3 percent addition of the BaSO₄ nanoparticles improved the properties of the polymer. The peak at 2116 cm⁻¹ indicated the interaction of the BaSO₄ nanoparticles with the polymer matrix when 3 percent of the BaSO₄ nanoparticles was added to the polymer matrix. The peak at 1568 cm⁻¹ was linked to the quinoid ring's (C=C) stretching modes.

The characteristic peak was observed at 1266 cm^{-1} after the addition of 5% of the BaSO_4 nanoparticles in the polymer matrix, as shown in Figure 2d, indicating that the 5 percent addition of the BaSO_4 nanoparticles increased the features of the polymer. The peak at 1628 cm^{-1} indicated the interaction of the BaSO_4 nanoparticles with the polymer matrix when 5 percent of the BaSO_4 nanoparticles was added to the polymer matrix. The peak at 1568 cm^{-1} was linked to the quinoid ring's (C=C) stretching modes.

The peak at 3511 cm^{-1} was, again, found by adding 7% of the BaSO_4 nanoparticles to the polymer matrix, as shown in Figure 2e, which was deep but not as wide as in the prior cases, indicating that the 7% addition of the BaSO_4 nanoparticles improved the polymer properties. Furthermore, the spectrum revealed that when 7% of the BaSO_4 nanoparticles are added to the polymer matrix, a peak at 1628 cm^{-1} indicates that the BaSO_4 nanoparticles are bound to the polymer matrix. The quinoid ring's (C=C) stretching modes were attributed to the peak at 1589 cm^{-1} .

Figure 2f shows the spectra of 10% of the BaSO_4 nanoparticles. It can be seen that due to the addition of 10% of the BaSO_4 nanoparticles in the poly(*o*-anisidine), a sharp and comparatively deep peak appeared at 3511 cm^{-1} , which showed the addition of 10% of BaSO_4 NPs, which increased the features of the poly(*o*-anisidine) differently. The peak that formed at 1626 cm^{-1} after the addition of 10% of the BaSO_4 nanoparticles to the poly(*o*-anisidine) matrix illustrated the binding of BaSO_4 nanoparticles to the polymer matrix. The quinoid-ring stretching modes (C=C) were exhibited at 1589 cm^{-1} [30].

3.2. UV-Visible Spectroscopy

The POA/ BaSO_4 nanocomposite was characterized to understand the absorption behavior of the POA/ BaSO_4 nanocomposite. To analyze the absorption behavior of composite materials, the materials were scanned in the wavelength range of 200–800 nm at the rate of 400 nm/min under a UV-visible spectrophotometer. The spectrophotometer was furnished with UV Winlab programming to record and analyze the information. A blank reference was used to conduct baseline correction on the spectrophotometer. The absorption spectra of the pure POA and POA/ BaSO_4 nanocomposites are shown in Figure 3. The significant absorption peak appeared at 273 nm, related to π - π^* aromatic C=C band transitions and n - π^* aromatic C=N band transitions. The *o*-anisidine monomer-to-monomer attachment was responsible for conjugation and polarity. The interaction of the BaSO_4 nanofiller and POA matrix resulted in a change in the absorption behavior of the composites. The absorption behavior of the composites was significantly different than that of the pure polymer, as shown in Figure 3a. There was a notable shifting of the absorption peak towards higher wavelengths, resulting in the marvel of the red shift at $\sim 520\text{ nm}$. Moreover, the absorption intensity of the composites was much higher than that of the pure polymer, indicating the role of barium-sulfate filler in improving the absorption properties of the POA/ BaSO_4 composites. The other composites also showed similar absorption behaviors, as depicted in Figure 3b–f. The absorption intensity was enhanced with the increase in the barium-sulfate-load percentage in the composites [17].

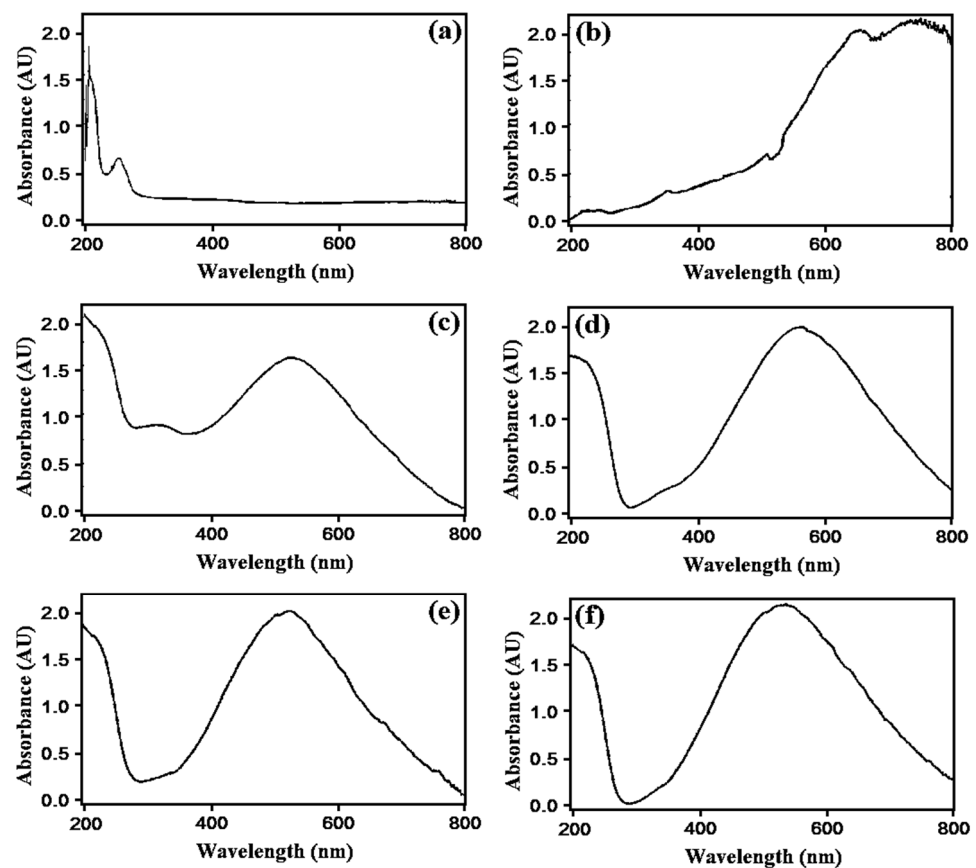


Figure 3. UV-visible spectra of (a) pure POA, (b) 1% of POA/BaSO₄, (c) 3% of POA/BaSO₄, (d) 5% of POA/BaSO₄, (e) 7% of POA/BaSO₄, and (f) 10% of POA/BaSO₄.

3.3. TEM Analysis

By using TEM micrograms at various magnifications to better examine the morphology of the BaSO₄ nanoparticles, Figure 4 was created. Due to their strong magnetic interaction and large surface area due to their nanoscale size, the produced BaSO₄ nanoparticles were found to be crystalline and include agglomerated irregular particles with an average size of 30–60 nm (Figure 4).

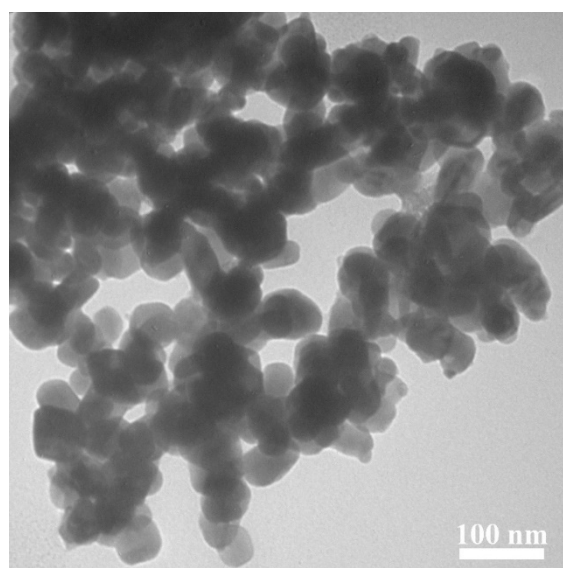


Figure 4. TEM micrograph of BaSO₄ nanoparticles.

3.4. Conductivity Test

The POA/BaSO₄ nanocomposites were subjected to the measurement of electrical conductivity by the conductivity meter. The electrical conductivity of the nanocomposites depends upon the properties of the individual components and also depends on the temperature factor.

Table 2 shows the electrical conductivity of POA at 1080 S/m. The electrical conductivities of the POA/BaSO₄ nanocomposites determined were lower than the pure POA. The nanocomposite with 1% of loading of the BaSO₄ nanoparticles showed conductivity at 992 S/m. Other nanocomposites containing 3%, 5%, 7%, and 10% of loading of BaSO₄ NPs exhibited conductivity at 919, 843, 784, and 578 S/m respectively (Figure 5). These results not only confirm the presence of nanoparticles but also show that the increase in the percentage of the BaSO₄ nanoparticles in the composites results in a decrease in the conductivity of the materials [17]. The addition of barium sulfate in poly(*o*-anisidine) allowed the composite properties to be tunable, which can be used for designing the sensor materials for future use.

Table 2. Scheme of conductivity test.

| Sr. No. | Sample Name | % BaSO ₄ NPs | Temperature (°C) | Conductivity (S/cm) |
|---------|----------------------------|-------------------------|------------------|---------------------|
| 1 | Poly(<i>o</i> -anisidine) | 0% | 25 °C | 1080 |
| 2 | POA/BaSO ₄ | 1% | 25 °C | 992 |
| 3 | POA/BaSO ₄ | 3% | 25 °C | 919 |
| 4 | POA/BaSO ₄ | 5% | 25 °C | 843 |
| 5 | POA/BaSO ₄ | 7% | 25 °C | 784 |
| 6 | POA/BaSO ₄ | 10% | 25 °C | 578 |

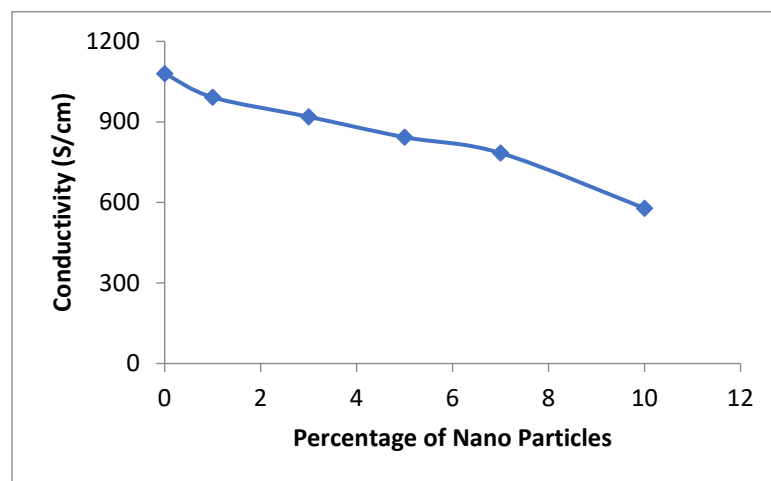


Figure 5. The plot of conductivity and nanoparticles' percentage relationship.

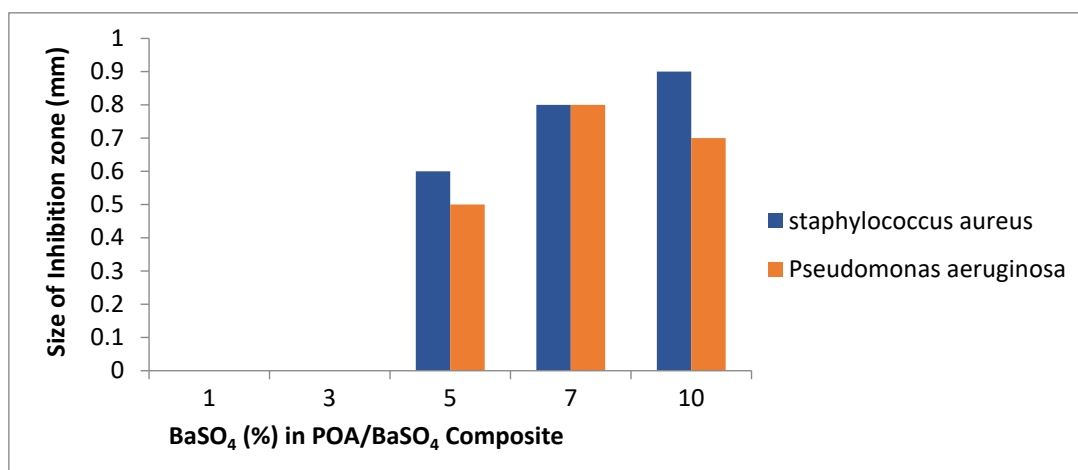
3.5. Disc-Diffusion Method

The synthesized poly(*o*-anisidine)/BaSO₄ nanocomposites were evaluated for their antibacterial activity against different strains of bacteria using the disc-diffusion technique. It was found that poly(*o*-anisidine)/BaSO₄ nanocomposites are effective for inhibiting the bacterial strains. The composites showed significant efficacy against *Pseudomonas aeruginosa* (Gram-negative) and *Staphylococcus aureus* (Gram-positive). The antibacterial activity of the BaSO₄ nanocomposites is noteworthy and reported in Table 3.

Table 3. Inhibition zone of antibacterial test of the BaSO₄ nanocomposite.

| Sample No. | Nanocomposite Concentrations (% w/w) | Inhibition Zone Diameter (mm) of <i>Staphylococcus aureus</i> | Inhibition Zone Diameter (mm) of <i>Pseudomonas aeruginosa</i> |
|------------|--------------------------------------|---|--|
| 1 | 1 | - | - |
| 2 | 3 | - | - |
| 3 | 5 | 0.6 | 0.5 |
| 4 | 7 | 0.8 | 0.8 |
| 5 | 10 | 0.9 | 0.7 |

The POA/BaSO₄ nanocomposite that inhibited *Pseudomonas aeruginosa* growth was found to be optimal at 7% (Table 3 and Figure 6). Similarly, *Staphylococcus aureus* growth was inhibited by the POA/BaSO₄ nanocomposites. The maximum inhibition was associated with 10% of the POA/BaSO₄ nanocomposites against Gram-positive bacteria (*Staphylococcus aureus*). Nanoparticles have a small size, a larger surface area than bulky particles, and better penetration; therefore, they have a greater bactericidal effect. The specific process by which nanoparticles enter bacteria is unclear; however, studies have shown that treating bacterial cultures with nanoparticles alters the shape of the membranes and significantly increases membrane permeability, impairing normal transport through the plasma membrane. Bacterial cells die when they are unable to manage the transport across the plasma membrane. It was believed that due to their small size, barium-sulphate nanoparticles enter the bacterial cell membrane and link to functional groups of proteins, causing denaturation. They are also hypothesized to cause bacterial cell death by interacting with phosphorus and sulphur compounds, such as DNA. Total bacterial inhibition was proportional to BaSO₄-nanoparticle concentrations [30]. It was found that the BaSO₄ nanoparticles have a significant antibacterial activity, which may be utilized for practical uses.

**Figure 6.** The graph shows the size inhibition zone of BaSO₄ nanoparticles in nanocomposites against load percentage.

4. Conclusions

The current study provides significant results regarding the antibacterial and conductivity properties of POA/BaSO₄ nanocomposites. Poly(*o*-anisidine)/BaSO₄ nanocomposites were synthesized by the oxidative polymerization of *o*-anisidine and variable percentages of BaSO₄ nanoparticles. The nanocomposites were tested by using different characterization techniques, i.e., FTIR, UV, and conductivity and disc-diffusion methods. The FTIR results show the strong communication among poly(*o*-anisidine) and BaSO₄ nanoparticles, and the UV-visible results indicate good absorption behavior. Moreover, the POA/BaSO₄ nanocomposites exhibited significant bactericidal potential against

Pseudomonas aeruginosa and *Staphylococcus aureus*, and a tunable electrical conductivity feature. Therefore, the versatile properties of poly(*o*-anisidine)/BaSO₄ nanocomposites identify these materials as future candidates for biomedical, electrical device, and sensor applications.

Author Contributions: The manuscript was written with the contributions of all authors. All authors have approved the final version of the manuscript.

Funding: This research was funded by Princess Nourah bint Abdulrahman University Researchers Supporting Project number (PNURSP2022R134), Princess Nourah bint Abdulrahman University, Riyadh, Saudi Arabia. The authors would like to thank the Deanship of Scientific Research at Umm Al-Qura University for supporting this work by grant code (22UQU4331312DSR06).

Institutional Review Board Statement: Not applicable.

Informed Consent Statement: Not applicable.

Data Availability Statement: The data will be available on request.

Acknowledgment: The authors extend their appreciation to the Research Center at AlMaarefa University for funding this work under TUMA project agreement number (TUMA-2021-22).

Conflicts of Interest: The authors declare no conflict of interest.

References

- Sebastian, J.; Samuel, J.M. Recent advances in the applications of substituted polyanilines and their blends and composites. *Polym. Bull.* **2019**, *77*, 6641–6669. <https://doi.org/10.1007/s00289-019-03081-7>.
- Thakur, S.; Patil, P. Enhanced LPG sensing-performance at room temperature of poly(*o*-anisidine)–CeO₂ nanocomposites. *RSC Adv.* **2016**, *6*, 45768–45782. <https://doi.org/10.1039/C6RA02955H>.
- Bonakdar, M.; Hosseini, S.R.; Ghasemi, S. Poly(*o*-Anisidine)/carbon nanotubes/graphene nanocomposite as a novel and cost-effective supercapacitor material. *Mater. Sci. Eng. B* **2021**, *267*, 115099. <https://doi.org/10.1016/j.mseb.2021.115099>.
- Alijani, H.; Abdouss, M.; Khataei, H. Efficient photocatalytic degradation of toxic dyes over BiFeO₃/CdS/rGO nanocomposite under visible light irradiation. *Diam. Relat. Mater.* **2022**, *122*, 108817. <https://doi.org/10.1016/j.diamond.2021.108817>.
- Ahmad, M.N.; Nadeem, S.; Javed, M.; Iqbal, S.; Khan, M.; Alsaab, H.O.; Awwad, N.S.; Ibrahim, H.A.; Mohyuddin, A. Photocatalytic Degradation of Yellow-50 Using ZnO/Polyorthoethylaniline Nanocomposites. *JOM* **2022**, *74*, 2106–2112.
- Rajkumar, R.; Vedhi, C. Preparation, characterization and anticorrosion behavior of Poly(*o*-anisidine)-SiO₂ nanocomposites on mild steel. *Mater. Today Proc.* **2022**, *48*, 169–173. <https://doi.org/10.1016/j.matpr.2020.06.048>.
- Sangjan, S.; Wisasa, K.; Deddeaw, N. Enhanced photodegradation of reactive blue dye using Ga and Gd as catalyst in reduced graphene oxide-based TiO₂ composites. *Mater. Today Proc.* **2019**, *6*, 19–23. <https://doi.org/10.1016/j.matpr.2018.05.071>.
- De Alvarenga, G.; Hryniewicz, B.M.; Jasper, I.; Silva, R.J.; Klobukoski, V.; Costa, F.S.; Cervantes, T.N.M.; Amaral, C.D.B.; Schneider, J.T.; Bach-Toledo, L.; et al. Recent trends of micro and nanostructured conducting polymers in health and environmental applications. *J. Electroanal. Chem.* **2020**, *879*, 114754. <https://doi.org/10.1016/j.jelechem.2020.114754>.
- Pandian, P.; Kalimuthu, R.; Arumugam, S.; Kannaiyan, P. Solid phase mechanochemical synthesis of Poly(*o*-anisidine) protected Silver nanoparticles for electrochemical dopamine sensor. *Mater. Today Commun.* **2021**, *26*, 102191. <https://doi.org/10.1016/j.mtcomm.2021.102191>.
- Jadoun, S.; Riaz, U.; Yáñez, J.; Pal Singh Chauhan, N. Synthesis, characterization and potential applications of Poly(*o*-phenylenediamine) based copolymers and Nanocomposites: A comprehensive review. *Eur. Polym. J.* **2021**, *156*, 110600. <https://doi.org/10.1016/j.eurpolymj.2021.110600>.
- Karbovnyk, I.; Klym, H.; Piskunov, S.; Popov, A.A.; Chalyy, D.; Zhydenko, I.; Lukashevych, D. The impact of temperature on electrical properties of polymer-based nanocomposites. *Low Temp. Phys.* **2020**, *46*, 1231–1234. <https://doi.org/10.1063/1.5100024>.
- Aksimientyeva, O.I.; Savchyn, V.P.; Dyakonov, V.P.; Piechota, S.; Horbenko, Y.Y.; Opainych, I.Y.; Demchenko, P.Y.; Popov, A.; Szymczak, H. Modification of Polymer-Magnetic Nanoparticles by Luminescent and Conducting Substances. *Mol. Cryst. Liq. Cryst.* **2014**, *590*, 35–42. <https://doi.org/10.1080/15421406.2013.873646>.
- Tsebriienko, T.; Popov, A.I. Effect of Poly(Titanium Oxide) on the Viscoelastic and Thermophysical Properties of Interpenetrating Polymer Networks. *Crystals* **2021**, *11*, 794. <https://doi.org/10.3390/cryst11070794>.
- Ahmad, M.N.; Hussain, A.; Anjum, M.N.; Hussain, T.; Mujahid, A.; Khan, M.H.; Ahmed, T. Synthesis and characterization of a novel chitosan-grafted-polyorthoethylaniline biocomposite and utilization for dye removal from water. *Open Chem.* **2020**, *18*, 843–849.
- Akyüz, D. rGO-TiO₂-CdO-ZnO-Ag photocatalyst for enhancing photocatalytic degradation of methylene blue. *Opt. Mater.* **2021**, *116*, 111090.
- Landa, R.A.; Calvino, J.J.; López-Haro, M.; Antonel, P.S. Nanostructure, compositional and magnetic studies of Poly(aniline)–CoFe₂O₄ nanocomposites. *Nano-Struct. Nano-Objects* **2021**, *28*, 100808. <https://doi.org/10.1016/j.nanos.2021.100808>.

17. Ahmad, M.N.; Rafique, F.; Nawaz, F.; Farooq, T.; Anjum, M.N.; Hussain, T.; Hassan, S.; Batool, M.; Khalid, H.; Shehzad, K. Synthesis of antibacterial poly (o-chloroaniline)/chromium hybrid composites with enhanced electrical conductivity. *Chem. Cent. J.* **2018**, *12*, 46.
18. Nadeem, S.; Iqbal, S.; Javed, M.; Ahmad, M.N.; Alsaab, H.O.; Awwad, N.S.; Ibrahim, H.A.; Ibrar, A.; Mohyuddin, A.; Haroon, S.M. Kinetic and Isothermal Studies on the Adsorptive Removal of Direct Yellow 12 Dye from Wastewater Using Propionic Acid Treated Bagasse. *Chem. Sel.* **2021**, *6*, 12146–12152.
19. Iqbal, S.; Bahadur, A.; Saeed, A.; Zhou, K.; Shoaib, M.; Waqas, M. Electrochemical performance of 2D polyaniline anchored CuS/Graphene nano-active composite as anode material for lithium-ion battery. *J. Colloid Interface Sci.* **2017**, *502*, 16–23.
20. Bahadur, A.; Iqbal, S.; Shoaib, M.; Saeed, A.J.D.T. Electrochemical study of specially designed graphene-Fe₃O₄-polyaniline nanocomposite as a high-performance anode for lithium-ion battery. *Dalton Trans.* **2018**, *47*, 15031–15037.
21. Iqbal, S.; Nadeem, S.; Bahadur, A.; Javed, M.; Ahmad, Z.; Ahmad, M.N.; Shoaib, M.; Liu, G.; Mohyuddin, A.; Raheel, M. The effect of Ni-doped ZnO NPs on the antibacterial activity and degradation rate of polyacrylic acid-modified starch nanocomposite. *Jom* **2021**, *73*, 380–386.
22. Lv, X.; Li, J.; Xu, L.; Zhu, X.; Tameev, A.; Nekrasov, A.; Kim, G.; Xu, H.; Zhang, C. Colorless to Multicolored, Fast Switching, and Highly Stable Electrochromic Devices Based on Thermally Cross-Linking Copolymer. *ACS Appl. Mater. Interfaces* **2021**, *13*, 41826–41835. <https://doi.org/10.1021/acsami.1c10089>.
23. Zaera, F. Designing Sites in Heterogeneous Catalysis: Are We Reaching Selectivities Competitive With Those of Homogeneous Catalysts? *Chem. Rev.* **2022**, *122*, 8594–8757. <https://doi.org/10.1021/acs.chemrev.1c00905>.
24. Wu, H.; Lin, S.; Chen, C.; Liang, W.; Liu, X.; Yang, H. A new ZnO/rGO/polyaniline ternary nanocomposite as photocatalyst with improved photocatalytic activity. *Mater. Res. Bull.* **2016**, *83*, 434–441. <https://doi.org/10.1016/j.materresbull.2016.06.036>.
25. Boutaleb, N.; Chouli, F.; Benyoucef, A.; Zeggai, F.Z.; Bachari, K. A comparative study on surfactant cetyltrimethylammoniumbromide modified clay-based poly(p-anisidine) nanocomposites: Synthesis, characterization, optical and electrochemical properties. *Polym. Compos.* **2021**, *42*, 1648–1658. <https://doi.org/10.1002/pc.25941>.
26. Peng, T.; Xiao, R.; Rong, Z.; Liu, H.; Hu, Q.; Wang, S.; Li, X.; Zhang, J. Polymer Nanocomposite-based Coatings for Corrosion Protection. *Chem. Asian J.* **2020**, *15*, 3915–3941. <https://doi.org/10.1002/asia.202000943>.
27. Elugoke, S.E.; Adekunle, A.S.; Fayemi, O.E.; Mamba, B.B.; Nkambule, T.T.I.; Sherif, E.-S.M.; Ebenso, E.E. Progress in electrochemical detection of neurotransmitters using carbon nanotubes/nanocomposite based materials: A chronological review. *Nano Sel.* **2020**, *1*, 561–611. <https://doi.org/10.1002/nano.202000082>.
28. Bahadur, A.; Saeed, A.; Shoaib, M.; Iqbal, S.; Anwer, S.J.J.o.A.P.S. Modulating the burst drug release effect of waterborne polyurethane matrix by modifying with polymethylmethacrylate. *J. Appl. Polym. Sci.* **2019**, *136*, 47253.
29. Nadeem Ahmad, M.; Anjum, M.N.; Nawaz, F.; Iqbal, S.; Saif, M.J.; Hussain, T.; Mujahid, A.; Farooq, M.U.; Nadeem, M.; Rahman, A. Synthesis and antibacterial potential of hybrid nanocomposites based on polyorthochochloroaniline/copper nanofiller. *Polym. Compos.* **2018**, *39*, 4524–4531.
30. Hussain, T.; Jabeen, S.; Shehzad, K.; Mujahid, A.; Ahmad, M.N.; Farooqi, Z.H.; Raza, M.H. Polyaniline/silver decorated-MWCNT composites with enhanced electrical and thermal properties. *Polym. Compos.* **2018**, *39*, E1346–E1353.
31. Merangmenla; Nayak, B.; Baruah, S.; Puzari, A. 1D copper (II) based coordination polymer/PANI composite fabrication for enhanced photocatalytic activity. *J. Photochem. Photobiol. A: Chem.* **2022**, *427*, 113803. <https://doi.org/10.1016/j.jphotochem.2022.113803>.
32. Pottle, V.D.; Shirsath, S.R.; Bhanvase, B.A.; Saharan, V.K. Sonochemical preparation of ternary rGO-ZnO-TiO₂ nanocomposite photocatalyst for efficient degradation of crystal violet dye. *Optik* **2020**, *208*, 164555. <https://doi.org/10.1016/j.ijleo.2020.164555>.
33. Hussain, A.; Ahmad, M.N.; Jalal, F.; Yameen, M.; Falak, S.; Noreen, S.; Naz, S.; Nazir, A.; Iftikhar, S.; Soomro, G.A. Investigating the Antibacterial Activity of POMA Nanocomposites. *Pol. J. Environ. Stud.* **2019**, *28*, 4191–4198.
34. Hussain, T.; Ahmad, M.N.; Nawaz, A.; Mujahid, A.; Bashir, F.; Mustafa, G. Surfactant incorporated Co nanoparticles polymer composites with uniform dispersion and double percolation. *J. Chem.* **2017**, *2017*, 1–6.
35. Monga, D.; Basu, S. Enhanced photocatalytic degradation of industrial dye by g-C₃N₄/TiO₂ nanocomposite: Role of shape of TiO₂. *Adv. Powder Technol.* **2019**, *30*, 1089–1098. <https://doi.org/10.1016/j.apt.2019.03.004>.
36. Li, X.; Peoples, J.; Yao, P.; Ruan, X. Ultrawhite BaSO₄ Paints and Films for Remarkable Daytime Subambient Radiative Cooling. *ACS Appl. Mater. Interfaces* **2021**, *13*, 21733–21739. <https://doi.org/10.1021/acsami.1c02368>.
37. Li, M.; Mann, S. Emergence of Morphological Complexity in BaSO₄ Fibers Synthesized in AOT Microemulsions. *Langmuir* **2000**, *16*, 7088–7094. <https://doi.org/10.1021/la0000668>.
38. Atone, M.S.; Dhoble, S.J.; Moharil, S.V.; Dhopte, S.M.; Muthal, P.L.; Kondawar, V.K. Luminescence in BaSO₄. *Eu Radiat. Eff. Defects Solids* **1993**, *127*, 225–230.
39. Cui, W.; Chen, L.; Li, J.; Zhou, Y.; Sun, Y.; Jiang, G.; Lee, S.; Dong, F. Ba-vacancy induces semiconductor-like photocatalysis on insulator BaSO₄. *Appl. Catal. B: Environ.* **2019**, *253*, 293–299. <https://doi.org/10.1016/j.apcatb.2019.04.070>.
40. Ugur, N.; Bilici, Z.; Ocakoglu, K.; Dizge, N. Synthesis and characterization of composite catalysts comprised of ZnO/MoS₂/rGO for photocatalytic decolorization of BR 18 dye. *Colloids Surf. A Physicochem. Eng. Asp.* **2021**, *626*, 126945. <https://doi.org/10.1016/j.colsurfa.2021.126945>.
41. Wu, G.; Zhou, H.; Zhu, S. Precipitation of barium sulfate nanoparticles via impinging streams. *Mater. Lett.* **2007**, *61*, 168–170. <https://doi.org/10.1016/j.matlet.2006.04.096>.

42. Birhan, D.; Tekin, D.; Kiziltas, H. Thermal, photocatalytic, and antibacterial properties of rGO/TiO₂/PVA and rGO/TiO₂/PEG composites. *Polym. Bull.* **2021**, *79*, 2585–2602. <https://doi.org/10.1007/s00289-021-03914-4>.
43. Aninwene, G.E.; Stout, D.; Yang, Z.; Webster, J.T. Nano-BaSO₄: A novel antimicrobial additive to pellethane. *Int. J. Nanomed.* **2013**, *8*, 1197–1205.
44. Ahmad, M.N.; Nadeem, S.; Hassan, S.U.; Jamil, S.; Javed, M.; Mohyuddin, A.; Raza, H. UV/VIS absorption properties of metal sulphate polymer nanocomposites. *Dig. J. Nanomater. Biostructures* **2021**, *16*, 1557–1563.